Extended x-ray absorption fine structure in $Ga_{1-x}Mn_xN$/SiC films with high Mn content

O. Sancho-Juan
Materials Science Institute, University of Valencia, Post Office Box 22085, E-46071 Valencia, Spain

O. Martínez-Criado
European Synchrotron Radiation Facility, 6 rue Jules Horowitz, F-38043 Grenoble, France

A. Cantarero* and N. Garro
Materials Science Institute, University of Valencia, Post Office Box 22085, E-46071 Valencia, Spain

M. Salomé and J. Susini
European Synchrotron Radiation Facility, 6 rue Jules Horowitz, F-38043 Grenoble, France

D. Olguín
Dept. de Física, Centro de Investigating Estudies Arauzados, 07300 Mexico DF, Mexico

S. Dhar and K. Ploog
Paul Drude Institute, Hausvogteiplatz 5-7, D-10117 Berlin, Germany

(Received 24 February 2011; revised manuscript received 1 April 2011; published 26 May 2011)

In this study, the local atomic structure of highly homogeneous $Ga_{1-x}Mn_xN$ alloy films ($0.03 < x < 0.09$) is analyzed by means of Mn and Ga *K*-edge extended x-ray absorption fine structure measurements. From the curve fitting, the structural parameters corresponding to the first two atomic shells surrounding both Ga and Mn atoms are reported. In the $Ga_{1-x}Mn_xN$ films, grown by molecular beam epitaxy, the Mn atoms are in tetrahedral configuration, independent of the Mn concentration; that is, they are in a substitutional site, Mn_{Ga}, in the wurtzite structure. A small increase in the interatomic distances has been found with increasing Mn content. The Debye-Waller factor does not show a significant trend as Mn content increases, which suggests the presence of short-range disorder in the GaN lattice. *Ab initio* calculations of the structural parameter for two different Mn concentrations are consistent with the experimental results.

DOI: 10.1103/PhysRevB.83.172103 PACS number(s): 61.05.cj, 71.55.Eq, 31.15.A−, 71.23.−k

I. INTRODUCTION

In the past two decades, diluted magnetic semiconductors (DMS) have attracted much attention because of their potential use in spintronics.[1,2] However, numerous investigations carried out on Mn-doped GaN have led to conflicting results.[3] At room temperature, ferromagnetism (FM) has been already reported in $Ga_{1-x}Mn_xN$,[4] while paramagnetism as well as antiferromagnetism has been also observed in $Ga_{1-x}Mn_xN$ thin films.[5–7] On the other hand, some reports on zinc-blend $Ga_{1-x}Mn_xN$ layers have given evidence of Mn-rich secondary phases,[8,9] whereas there were no signs of metal clustering effects from nanocrystalline hexagonal $Ga_{1-x}Mn_xN$ films.[10] A recent *ab initio* calculation shows an antiferromagnetic behavior in both zinc-blend and wurtzite $Ga_{1-x}Mn_xN$ nanocrystals.[11] Therefore, in order to clarify the wide variety of behaviors, it is still crucial to study the local structure surrounding the different atoms in the host lattices by means of extended x-ray absorption fine structure (EXAFS) technique. So far, depending on the Mn content and growth conditions, former EXAFS studies have shown different findings concerning the lattice distortions, interatomic lengths, and Debye-Waller (DW) factors. Although most of the reports provide direct evidence of Mn occupation of Ga site in the host lattice, a summary of various results are listed here: (i) In nanocrystalline $Ga_{1-x}Mn_xN$ films ($x \leqslant 0.18$) prepared by ion-assisted deposition from the Mn and Ga *K* edges the radial distances to the first and second nearest shells are equal within the fitting uncertainty, and both agree with the shell radii around the Ga in Mn-free crystalline GaN.[10] (ii) The results above contrast with EXAFS measurements taken on single-crystalline $Ga_{1-x}Mn_xN$ films, which exhibit a lengthening of the Mn-N bond by almost 5% for $x = 0.057$.[12] (iii) From $Ga_{1-x}Mn_xN$ films grown on 6H-SiC (0001) substrates by molecular beam epitaxy (MBE), two distinct Mn sites were reported though first principle calculations indicated that at high concentrations Mn preferentially populates Ga sites neighboring N split interstitial defects.[13] (iv) In bulk $Ga_{1-x}Mn_xN$ crystals, the observed discrepancies between the experimental EXAFS data and the simulation results were attributed either to the lattice relaxation around Mn atoms or to the admixture of nonsubstitutional Mn sites by clustering effects or precipitates.[14] (v) Finally, using $Ga_{1-x}Mn_xN$ layers grown by MBE on (0001) sapphire substrates, an EXAFS study indicated that the nonsubstitutional Mn is not present in the form of Ga_xMn_y clusters but most likely in the form of interstitials.[15]

In this paper, to examine Mn-dependent local structural changes, we apply the EXAFS technique to highly homogeneous GaN samples with Mn contents up to ∼9%, estimated from x-ray fluorescence spectroscopic analysis.[16] Up to now, most of the produced materials were grown on the naturally appealing Al_2O_3 substrate. Here, several $Ga_{1-x}Mn_xN$ epilayers

grown by MBE on 2H- and 4H-SiC (0001) substrates will be studied. Details on the sample growth, as well as preliminary x-ray absorption results, can be found elsewhere.[4,16,17]

II. EXPERIMENTAL SETUP

In x-ray fluorescence detection mode, the EXAFS spectra were recorded at room temperature around the Mn and Ga K edges: 6.550 and 10.363 keV, respectively. The measurements were carried out at the soft and hard x-ray microprobes, beam lines ID21 and ID22, of the European Synchrotron Radiation Facility (ESRF). Both stations, operating in complementary energy ranges, are equipped with insertion device sources, Si mirrors for harmonics rejection, and fixed-exit double Si (111) crystal monochromators ($\Delta E/E \approx 10^{-4}$). At ID21, the monochromatic beam is focused on the sample surface with up to 500 nm^2 beam size using chromatic Au Fresnel zone plates (photon flux $\approx 10^9$ phot/s at Mn K edge). At ID22, the spatial resolution of 1.5×3.5 μm^2 is reached by achromatic Kirkpatrick-Baez Si mirrors (photon flux $\approx 10^{11}$ phot/s at Ga K edge). The intensity of the incident x-ray beam at ID21 is detected with a Si diode associated to a fluorescence foil, whereas at ID22 an ionization chamber filled adequately with a gas mixture monitors the photon flux. Finally, single-element solid-state detectors with Si(Li) and Ge crystals are used to collect the characteristic x-ray fluorescence lines at ID21 and ID22 respectively. The data were recorded with the sample surface normal **n** parallel to the polarization vector ε of the synchrotron radiation ($\varepsilon \parallel \mathbf{n}$). The measurement conditions included an energy step of 0.5 eV and integration times were determined by the counting statistics. The data analysis was done using the XAFS-code-based programs ATHENA and ARTEMIS.[18]

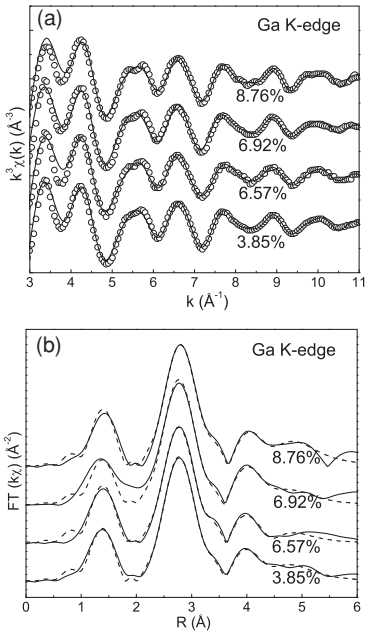

FIG. 1. (a) k^3-weighted Ga K-edge EXAFS of $Ga_{1-x}Mn_xN$ samples with different Mn contents. The spectra are compared to their best fits. The data were recorded with the polarization vector of the synchrotron radiation aligned parallel to the sample surface normal ($\varepsilon \parallel \mathbf{n}$). (b) Non-phase-corrected Fourier transform magnitudes of the EXAFS spectra over a k range of 2–15 Å^{-1}.

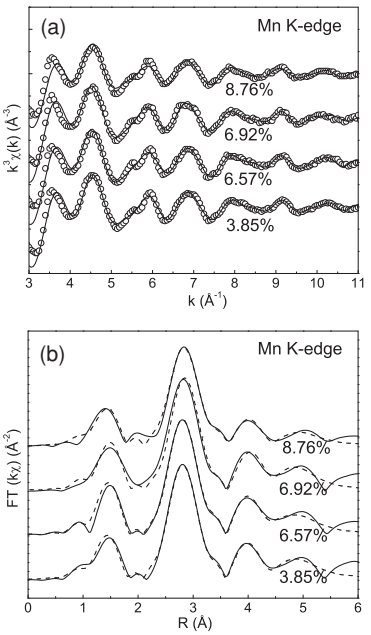

FIG. 2. (a) k^3-weighted Mn K-edge EXAFS of $Ga_{1-x}Mn_xN$ samples with different Mn contents. The spectra are compared to their best fits. The data were recorded with the polarization vector of the synchrotron radiation aligned parallel to the sample surface normal ($\varepsilon \parallel \mathbf{n}$). (b) Non-phase-corrected Fourier transform magnitudes of the EXAFS spectra over a k range 2–15 Å^{-1}.

III. RESULTS AND DISCUSSION

Accompanied by their best fits, the k^3-weighted Ga and Mn K-edge EXAFS oscillations $\chi(k)$ extracted from the room-temperature raw data are shown in Figs. 1(a) and 2(a) for different Mn contents. Note that the noise level was much lower than the oscillation amplitude for all the spectra for $k < 11$ Å^{-1}. The data analysis was carried out by *ab initio* modeling of the absorption cross section by the FEFF code.[19] the theoretical backscattering amplitudes and phase shifts for all single- and multiple-scattering paths were calculated using hexagonal GaN model clusters ($a = 3.18$ Å and $c = 5.168$ Å) in the wurtzite packed structure; the bond configuration is tetrahedral, with equal interatomic distances, in accordance with our previous findings.[16] The ARTEMIS routine was exploited to fit data in R space within the window of [0–4 Å, which included the first and second coordination shells. Based on previous x-ray diffraction data,[4] a fixed coordination of four N nearest-neighbor atoms and 12 Ga next-nearest-neighbor atoms, features common to wurtzite or zinc-blend GaN sequence, was applied. We have fitted the interatomic distances R_i and the relative mean square deviations σ_i^2 of the different atomic shells. The values of the structural parameters extracted from the curve fits, R_i and σ_i^2, are reported in Table I. Figures 1(b) and 2(b) show the corresponding magnitude of the Fourier transforms (FTs) of the Ga and Mn K-edge EXAFS functions for different Mn contents in the $Ga_{1-x}Mn_xN$ samples.

In good agreement with the uniform x-ray fluorescence maps,[16] no evidence of randomly distributed variations of

TABLE I. Summary of the parameters deduced from the analysis of the EXAFS spectra of the $Ga_{1-x}Mn_xN$ films investigated in this work at the Ga and Mn *K* edges. In parentheses, we show the uncertainty of the last digit obtained from the analysis.

x (%)	R_{Ga-N} (Å)	σ^2_{Ga-N} 10^{-3} (Å^2)	R_{Ga-Ga} (Å)	σ^2_{Ga-Ga} 10^{-3} (Å^2)	R_{Mn-N} (Å)	σ^2_{Mn-N} 10^{-3} (Å^2)	R_{Mn-Ga} (Å)	σ^2_{Mn-Ga} 10^{-3} (Å^2)
3.85	1.939(9)	3.5(8)	3.188(8)	5.1(4)	1.969(10)	6.5(1.2)	3.200(7)	6.5(3)
6.57	1.941(8)	2.6(7)	3.194(8)	2.5(4)	1.983(11)	4.0(1.1)	3.207(8)	6.2(4)
6.92	1.96(2)	5(2)	3.198(16)	4.8(8)	1.986(13)	5.0(1.4)	3.211(9)	6.5(5)
8.76	1.943(9)	2.9(9)	3.201(9)	5.2(4)	1.97(2)	9(2)	3.219(12)	7.6(5)

the short-range order was observed among EXAFS spectra collected at different sample points within the length scale of the beam size. A qualitative comparison of both *K*-edge spectra shows a close correspondence among the respective oscillations at different Mn contents. Contrary to a previous report on MBE $Ga_{1-x}Mn_xN$ layers,[15] where the Mn atoms are located on interstitial positions, our results strongly suggest a substitutional incorporation of this transition metal in the GaN lattice.[10] Around the Ga *K* edge, the FT spectra closely resemble those of the the Mn-free GaN lattice.[20] In general, the EXAFS spectra reveal almost no change in amplitude as the Mn fraction increases. In the lower panel of Fig. 1, a small shift is found in the positions of the Ga-N and Ga-Ga peaks (see Table I). In the lower panel of Fig. 2, we observe a small shift in the position of the Mn-Ga peak; however, in the position of the Mn-N peak there is no clear evidence of a shift (Table I).

Based on the structural parameters obtained from the curve fitting and listed in Table I, Fig. 3 (upper panel) illustrates an overview of the experimental values for the interatomic distances as a function of the Mn concentration. The interatomic spacings appear to vary little with the Mn composition, consistent with other report where slight interatomic length distortions were observed.[10] Within the

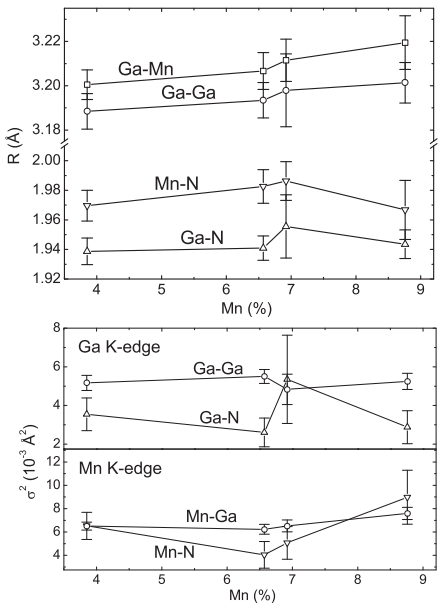

FIG. 3. Upper panel: Neighbor distances in GaMnN films as a function of the Mn content. Lower panel: Debye-Waller factors for different doping levels in GaMnN.

fitting uncertainty, compared to bulk GaN crystal, [21] in our epitaxial $Ga_{1-x}Mn_xN$ layers the neighbor distances are found to be in the same range: $R_{Ga-N} = 1.95$ Å and $R_{Ga-Ga} = 3.184$ Å, virtually equal to the wurtzite lattice parameter of the bulk GaN structure. From the structure determination on GaN single crystals,[22] $R_{Ga-N} = 1.956$ Å ($R_{Ga-N} = 1.949$ Å in the apical direction) and $R_{Ga-Ga} = 3.190$ Å. However, from a quantitative comparison, the (Mn-N) and (Mn-Ga) distances are systematically ~0.03 Å longer than the (Ga-N) and (Ga-Ga) separation in all $Ga_{1-x}Mn_xN$ epilayers. The observed differences could arise from additional doping-induced effects. The possibility of Mn clustering defects might play an important role. In a previous study, [4] the existence of nanometric clusters (2–5 nm) of unknown origin was shown by transmission electron microscopy in the sample with the highest Mn content. Actually, this sample is the only one presenting ferromagnetism, as previously reported by Dhar *et al.*[4] This is in agreement with a theoretical work of Kang *et al.*[23] They show how, in the balance between exchange and superexchange interaction, ferromagnetism appears for a Mn concentration larger than 6% and also that this high concentration of Mn favors the existence of metallic Mn clusters, contributing also to the FM. On the other hand, by Raman scattering measurements, in addition to the strain-induced shifts consistent with the values of R_{Ga-Ga} listed in Table I, Mn-induced lattice disorder has also been identified.[24] In an EXAFS study, a similar finding was recently reported by Baik *et al.* from (Ga,Mn)N nanowires.[25]

Although its variation could be too noisy to be meaningful as structural parameters, the DW factors reported in Fig. 3 (lower panel) support the general trend of our previous findings. In a previous x-ray absorption investigation,[8] the high level of Mn doping resulted in a considerable strain of the first atomic shell, corresponding to a large number of nitrogen defects in the GaN lattice. In the same way, the distortion of the second-nearest-neighbor shell around the Ga atoms in GaN has been attributed to local lattice relaxation around the nitrogen vacancies.[20] Kuroda and co-workers, on the other hand, report a clear contrast between the precipitation of a perovskite compound $GaMn_3N$ at compositions higher than 1.7% and the single phase of the wurtzite $Ga_{1-x}Mn_xN$ at lower Mn contents.[26] Therefore, the parallel incorporation of doping-induced defects with the Mn level cannot be ruled out.

In order to deepen in the variation of the interatomic distances we have performed an *ab initio* calculation of GaN + Mn using the full potential linear augmented plane-wave method as implemented by Blaha *et al.* in the WIEN2K code.[27] In order to simulate the Mn content we constructed

TABLE II. Calculated first- and second-neighbor distances in $Ga_{1-x}Mn_xN$. The calculations have been performed using $2 \times 2 \times 1$ and $3 \times 3 \times 2$ supercells with one Mn atom/cell, equivalent to 6.25% and 1.39% of Mn content.[16] The symbol *ap* refers to the apical position. All distances are given in Å. The uncertainties in the theoretical data are of the order of 0.002 Å.

x	$R_{Ga-N}(ap)$	R_{Ga-N}	$R_{Mn-N}(ap)$	R_{Mn-N}	R_{Mn-Ga}	R_{Ga-Ga}	R_{N-N}
0	1.948	1.951				3.183	3.183
1.39	1.980	2.007	1.947	1.920	3.226	3.235	3.234
6.25	1.991	2.016	1.948	1.921	3.232	3.242	3.145

two supercells, consisting of $2 \times 2 \times 1$ and $3 \times 3 \times 2$ wurtzite cells, equivalent to 6.25% and 1.39% of Mn content.[16] The positions of all atoms were optimized within the supercell. To guarantee the convergence, we used a cutoff of 10 Ry and 50 k points in the irreducible part of the Brillouin zone. In Table II, we show the different interatomic distances obtained from the optimized structures and also the calculations performed for bulk GaN ($x = 0$). The lattice parameters for bulk GaN agree quite well with the experiment.[22] Although from the calculations we have four confident figures after the decimal point, we have kept only three figures since the experimental data have larger errors. By comparing the Ga-N bond distances with increasing Mn content, we obtain similar trends as in the experiment: The interatomic distances increase slightly with Mn content as in the experiment, but in the theory we are able to distinguish the Ga-N in the apical (z) direction from the other three bonds below the xy plane. The N in the apical direction is closer to the Ga. Concerning the Mn-N bond distance, the calculated values are smaller than the experimental ones, and they do not vary with increasing Mn content. The coordination of N around Mn corresponds to a distorted tetrahedral, where the Mn-N distance in the z direction is nearly 0.03 Å larger than the other three bonds. In the fitting to the experimental data, we neglected the possible distortion, considering the N in the vertices of a regular tetrahedral with center in the Mn atom. The second neighbor Ga-Ga and Mn-Ga bond distances are also of the same order and increase slightly with Mn content. Finally, the N-N second neighbor distance, not measured in the experiment, shows a decrease with Mn content, consistent with the increase of Ga-N distances. Overall, there is a small increase of the volume with increasing Mn content, which can be interpreted as an increase of the internal pressure due to the larger radius of Mn as compared to Ga. The increase of the volume is consistent with the larger covalent radius of Mn (1.39 or 1.61 Å, depending on the spin state) as compared to Ga ($r = 1.22$ Å).[28]

IV. CONCLUSIONS

In conclusion, the local structure of $Ga_{1-x}Mn_xN$ layers grown by molecular beam epitaxy has been investigated by x-ray absorption microspectroscopy. With Mn content ranging from 3% up to 9%, the films are found to be highly uniform on the micrometer scale with respect to the short-range order. EXAFS measurements taken around Mn and Ga K edges are consistent with the Mn replacing Ga atoms substitutionally in the host GaN lattice. Around the Mn-absorbing atoms, the nearest-neighbor interatomic lengths were slightly larger than those around the Ga atoms. Although the extracted Debye-Waller factor appears to be essentially composition independent, the results suggest that Mn incorporation induces a small but detectable static disorder.

ACKNOWLEDGMENTS

This work has been partially supported by the Ministerio de Ciencia e Innovación of Spain (Grant MAT2009-10350), and the European Synchrotron Radiation Facility. We thank the computing facility at the Red Española de Supercomputación (Tirant).

*andres.cantarero@uv.es

[1] R. P. Davies *et al.*, Chem. Eng. Comm. **196**, 1030 (2009).
[2] K. S. Burch *et al.*, J. Magn. Magn. Mater. **320**, 3207 (2008).
[3] S. J. Pearson *et al.*, J. Phys. Condens. Matter **16**, R209 (2004).
[4] S. Dhar *et al.*, Appl. Phys. Lett. **82**, 2077 (2003).
[5] F. Takano *et al.*, Physica B **376–377**, 658 (2006).
[6] G. M. Dalpian and S.-H. Wei, J. Appl. Phys. **98**, 083905 (2005).
[7] S. Granville *et al.*, Phys. Rev. B **81**, 184425 (2010).
[8] B. He *et al.*, Appl. Phys. Lett. **88**, 051905 (2006).
[9] K. Biswas *et al.*, Appl. Phys. Lett. **89**, 132503 (2006).
[10] S. Granville *et al.*, J. Appl. Phys. **100**, 084310 (2006).
[11] C. Echeverría-Arrondo *et al.*, Phys. Rev. B **82**, 205419 (2010).
[12] M. Sato *et al.*, Jpn. J. Appl. Phys., Part 1 **41**, 4513 (2002).
[13] D. J. Keavney *et al.*, Phys. Rev. Lett. **95**, 257201 (2005).
[14] R. Bacewicz *et al.*, J. Phys. Chem. Solids **64**, 1469 (2003).
[15] G. Thaler *et al.*, Appl. Phys. Lett. **84**, 1314 (2004).
[16] O. Sancho-Juan *et al.*, J. Phys. Condens. Matter **21**, 295801 (2009).
[17] O. Sancho-Juan *et al.*, Phys. Status Solidi B **243**, 1692 (2006).
[18] B. Ravel and M. Newville, J. Synchrotron Radiat. **12**, 537 (2005).
[19] A. L. Ankudinov *et al.*, Phys. Rev. B **58**, 7565 (1998).
[20] M. Katsikini *et al.*, J. Synchrotron Radiat. **6**, 561 (1999).
[21] F. d'Acapito *et al.*, Phys. Rev. B **66**, 205411 (2002).
[22] H. Schulz and K. H. Thiemann, Solid State Commun. **23**, 815 (1977).
[23] J. Kang *et al.*, J. Supercond. **18**, 55 (2005).
[24] A. Cantarero *et al.* (unpublished).
[25] J. M. Baik *et al.*, Appl. Phys. Lett. **89**, 152113 (2006).
[26] S. Kuroda *et al.*, Phys. Status Solidi B **240**, 443 (2003).
[27] P. Blaha K. Schwarz, G. Madsen, D. Kuasnicka, and J. Witz, [http://www.wien2k.at/].
[28] B. Cordero *et al.*, Dalton Trans. **2008**, 2832 (2008).